“Tribological solicitations” of piezoelectric inertia motors by means of in situ tribotesting and 3rd body flow framework

Fabien Dubois, Aurélien Saulot, Christian Belly, Yves Berthier

Version of Record: https://www.sciencedirect.com/science/article/pii/S0043164817312887
Manuscript_311bb57c39e685c1c5dae17abc96b2b8

"Tribological solicitations" of piezoelectric inertia motors by means of *in situ* tribotesting and 3rd body flow framework

Fabien Dubois [a, b,*], Aurélien Saulot [a], Christian Belly [b], Yves Berthier [a]

[a] *INSA de Lyon, LaMCoS UMR CNRS 5259, F-69621, France*
[b] *Cedrat Technologies S.A., 59 Chemin du vieux chêne, Innovallée, 38246 Meylan Cedex, France*

Abstract

In piezoelectric inertia motors, friction is not a synonymous of energy loss but is the source of motion. Their performances are thus prone to wear and friction coefficient variation. To address these issues, this paper first aims at improving the understanding of tribological solicitations by means of a dedicated *in situ* tribotesting while exploiting the 3rd body flow framework. Beyond the introduction of transparent glass pins to see inside the contact in operation, the key of this work is to consider both the mechanism effect and the friction couple. As a result, a solution has been proposed to multiply the motor lifetime by more than ten while keeping stable speed performances, and, above all, without multiplying tests with numerous friction materials.

Keywords: Dynamic *in situ* tribotesting, 3rd body flows, stick-slip, piezoelectric inertia motors, Si_xO_y-coated Ti-6Al-4V *vs*. fibreglass filled composite contact.

* Corresponding author.
E-mail address: dubois.fabien38@gmail.com (F. Dubois)

1. Introduction

Piezoelectric inertia motors [1] are based on the combination of two energy conversion mechanisms. First, an electric signal is converted into mechanical deformations by means of piezoelectric inverse effect [2]. Second, the resulting asymmetric vibratory oscillations are converted into linear or rotary displacements by means of a friction interface, relying on stick and slip alternations. By this way, a centimetric stroke may be reached with a resolution down to subnanometer [3]. Therefore, inertia motors are used in many applications such as laboratory nano-positioning [4], general public anti-blur camera [5], multi-degree of freedom applications [6], or robotic [7], even in harsh environments such as cryogenic [8], ultra-high-vacuum [9] and non-magnetic [10].

But, as friction occurs to ensure the motion of a payload, the performances of these motors such as wear rate and lifetime are consequently inherent to tribological solicitations: the employed material couple, the surface conditions, the environment and the motor mechanism itself. Understanding these solicitations as a whole is necessary to improve motor performances.

Faced with the numerous parameters involved in the design of piezoelectric motors (*e.g.* piezoelectric actuator model, normal load configuration, guidance, actuation frequency [11]), and the stick-slip bound tribological solicitations (*e.g.* sliding velocity, contact area, surface energy [12]), it is complicated to analyse a given material couple exclusively from bibliographical considerations. Likewise, Discrete Element Modelling (DEM) could be a fruitful approach for getting the dynamic behaviour of a contact interface at a local scale by describing flows of solid particles as granular elements [13]. However, calculations remain too time-consuming to be considered in this work. It becomes necessary to carry out an experimental approach based on tribometry. To do so, it requires beforehand a decryption of contact life with a strict framework. Both tribological triplet and 3rd body flows approaches have been adopted to get contact life through the tribological circuit (Fig. 1, [14]).

Assessing tribological solicitations bound to a given material couple may depend on employed measurement method and contact conditions, as highlighted during the VAMAS project [15]. Bergander et al. also emphasized that even reciprocating tribometer, closer to the macroscopic motion of inertia motor, is not close enough to the final application to provide valuable results [16]. Likewise, Blau et al. highlighted that friction coefficient can change significantly with measurement conditions [17]. Actually, through the tribological analysis, contact conditions proper to the mechanism are equally important as the material couple itself.

But, considering the link between mechanism and contact conditions is not the only point. Another difficulty in studying friction contact is the lack of measurable *in situ* data without being invasive. To do so, different approaches have been proposed. Some of them were brought by the elasto-hydrodynamic studies (reviewed in [18]) at nano-scale level but they reach limits in dry contacts. Another approach consists in correlating acoustic emission signals and wear mechanisms [19]. Although this method is the less invasive, this is quite new and does not make it possible to distinguish different wear mechanisms if they occur at the same time. It is also possible to carry out stopped tests with unload/measure/load sequences [20] but 3rd body distribution may change inside the contact [21]. So, conducting direct *in situ* tribometry through transparent bodies appears to be a beneficial approach as reflected in numerous previous work [22-33]. Although using a transparent material can lead to change in friction behaviour [24, 34], this makes it possible to observe 3rd body creation and motion inside the contact [24-27, 30, 31, 35]. The evolution of the created 3rd body layer may be then linked to the measured motor performances [27, 28]. Simultaneously, friction materials used in real motors are also tested. All gathered information provides the scenario of the contact life.

So, to understand the tribological solicitations, an experimental approach is carried out, close to the operating conditions of the studied motors with both transparent and real friction interfaces. The practical objective is to improve the tribological performances of inertia motor, by both increasing the lifetime while maintaining a stable friction coefficient.

The paper firstly introduces the experimental approach from the dedicated test bench to the 3rd body framework and the test procedure (section 2). This framework enabled to compare - by means of *in situ* and *post mortem* observations - different tests with a same methodology to propose systematic analyses, whose conclusions would be less dependent on the observer (section 3). Final sections detail the main outcome and some points of discussion (section 4) as well as a summary and a conclusion (section 5).

Nomenclature

Flow Q_s^i	internal source flow characterizes the origin of 3rd body inside the contact. It is obtained by detachment of particles from the degradation of the 1st bodies.
Flow Q_s^e	external source flow is obtained by artificial external supply. Particles constituting this flow can come from different origins: particle detachment from other parts of the mechanism, particles from environment.
Flow Q_i	internal flow characterizes the motion of 3rd body inside the contact.
Flow Q_e	external flow characterizes particles ejected from the contact. This flow is divided into two subflows: Q_r and Q_w.
Flow Q_r	recirculation flow corresponds to the flow of particles reintroduced into the contact after ejection.
Flow Q_w	wear flow: is composed of particles that will never be reintroduced into the contact after ejection.
Site S_0	mechanism has its own kinematics and imposes contact conditions.
Sites S_1 and S_5	bulk of 1st bodies.
Sites S_2 and S_4	so called screens because they prevent adhesion by screening the surface forces.
Site S_3	3rd body. S_2, S_3, and S_4 sites do not necessarily exist at the same time.
Mode M_1	elastic deformation corresponds to a reversible mechanism. All solids deform elastically and all deformations can account for some velocity accommodation.
Mode M_2	normal rupture is non-reversible. It is not a velocity accommodation mechanism *per se* since a crack does not accommodate displacement or velocity alone but it allows for much greater deformation through other modes.
Mode M_3	shearing is also non-reversible.
Mode M_4	rolling is also non-reversible. It corresponds to the formation of rolls during friction.

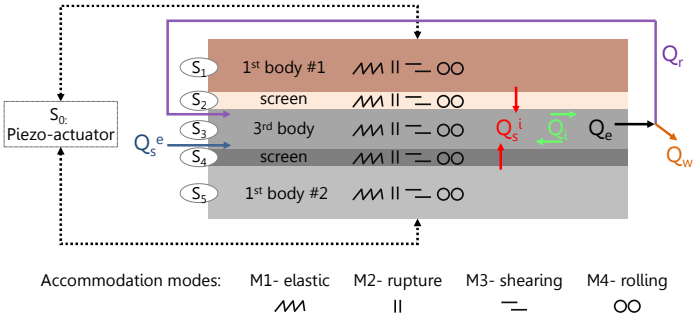

Fig. 1. 3rd body formalism. The tribological triplet is composed of a mechanism, the rubbing 1st bodies and the 3rd body particles. Resulting tribological circuit - described in nomenclature and used in this work - is characterized by (i) solid particle flows and (ii) velocity accommodation mechanisms decomposed in location sites S_i and accommodation modes M_j [14].

2. Experimental approach

This section reminds the key features of the dedicated tribometer, introduced in [36], aiming at carrying out the direct *in situ* analyses (section 2.1). Experimental framework and material test procedure are also detailed (section 2.2 and 2.3).

2.1. Test bench

This test bench has been designed to be as close as possible to the operating conditions of the final application (Fig. 2). Thus, a piezoelectric actuator generates the tangential motion and a spring preloads the friction contact to get closer to the behaviour of a real motor (section 2.1.1). This actuator triggers stick-slip transitions, responsible for the relative displacement creation (section 2.1.2) between the 1st bodies (section 2.1.3). Relative instrumentation is reminded in section 2.1.4.

2.1.1. Mechanism characterisation

The static and dynamic features of the test bench (Fig. 2-a) as well as mounting conditions will impact the 3rd body flows and should be considered upon the analysis of tribological solicitations.

Static features such as material properties and kinematics are key features to characterize the tribological solicitations. They are detailed in Table 1.

Dynamic characterisation makes it possible to determine which degrees of freedom have the most influence during actuation. For instance, the theoretical trajectory of the pin is a linear reciprocating motion along the guidance axis ($\vec{x}$ axis on Fig. 2). However, pivotal motion at the contact scale is expected because of the cylinder-on-flat geometry.

Third, mounting conditions such as screwing or gluing may play a role. For instance, during assembly, oscillation mass is screwed to actuator (Fig. 2-b). As a consequence, a torque is applied at the contact location. To minimize it, pin and pad are glued under preload to oscillation mass and moving mass respectively. By this way, glue layer may accommodate this aforementioned torque.

These points will be further tackled once the tribological analysis has been carried out (section 4.2).

Table 1. Material properties and contact conditions

Materials	**Young's modulus [GPa]**	**Poisson ratio**
Fibreglass composite	14	0.39
Ti-6Al-4V	114	0.33
B270 glass	72	0.22
Kinematics	**Stick-slip**	
Actuation period [ms]	1.25	
Delay period [ms]	3.75	
Step amplitude [µm]	100 (+/-40)	
Total stroke [mm]	+/- 45	
Mean speed [mm/s]	18	
Contact conditions		
Geometry [mm x mm]	R30x10- cylinder pin on flat pad	
Contact width [µm]	70	

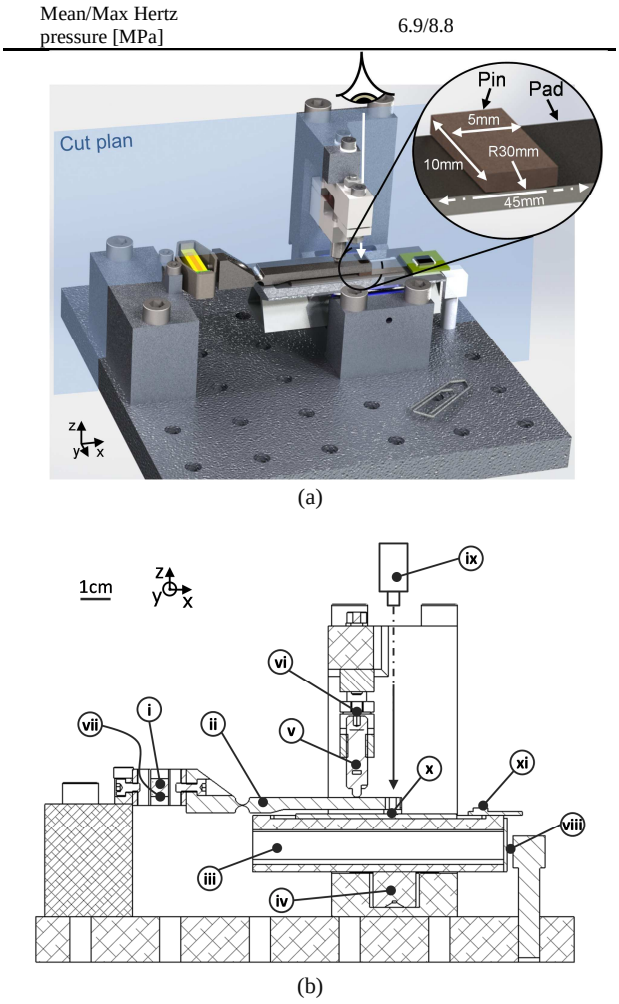

Fig. 2. Tribometer setup. (a) illustration and (b) Cut plan. (i) Piezoelectric actuator linked to (ii) the Oscillating Mass (OM) in friction contact with (iii) the Moving Mass (MM). (iv) Guiding and lift are provided by air bearings. (v) Normal load is provided by a spring contained in a screw. (vi) Applied normal force is measured by a strain gauge mounted on specific deformable test body. (vii) A second strain gauge is mounted on actuator to get the displacement of the actuator and so of the OM. (viii) Eddy current sensor is used to get the displacement of the MM. Sensor sampling is set to 100kHz. (ix) Camera (0.1Hz sampling) or high-speed camera (30kHz sampling). Extra light is provided by LED light to make high speed camera acquisition possible without harming contact. (x) Observation window to see through pin. (xi) An accelerometer is mounted on MM to get tangential force and so friction coefficient.

2.1.2. Stick-slip actuation

Stick-slip phenomenon [12] is often described as a dynamic instability and a source of noise [37]. In piezoelectric inertia motor, stick-slip is no more synonym of energy loss but becomes the source of motion [38]. It consists in exploiting an asymmetric vibration generated by the piezoelectric actuator:

- First, the piezoelectric ceramic is in a neutral state with no voltage applied.
- Second, voltage order slowly increases. Piezoelectric ceramic slowly expands, driving the Oscillating Mass (OM) and so the Moving Mass (MM) with a low acceleration (Fig. 2-b). An external force is created on MM. As long as it remains smaller than the static friction force, both OM and MM stick and move together. This is the stick phase.
- Third, voltage order quickly comes back to neutral state. Piezoelectric ceramic quickly contracts, and pulls OM with a high acceleration. An external force, higher than the static friction force, is applied on MM. OM goes back to its initial states whereas MM stands still with respect to the ground, by means of its inertia. This is the slip phase.
- At last, piezoelectric ceramic is in a neutral state again with no voltage applied.

By continuously alternating stick and slip phases, step movement appears and MM keep moving in a large range stroke. If the shape of the voltage is in a reverse order, the moving mass will travel to the opposite direction.

2.1.3. Initial state of friction 1st bodies

1st bodies in the considered motors are a fibreglass filled polymer and a Si_xO_y-coated Ti-6Al-4V.

It is easier to manufacture large metal parts with precise tolerances. So, initial pin is in fiberglass filled polymer material and pad is in Ti-6Al-4V. However, it seemed interesting here to test both orientations so reciprocal counterparts were also manufactured.

Ti-6Al-4V is used because of both its biocompatibility properties [39] and MRI compatibility [10] making it possible to address medical application fields. Due to its cold-welding propensity [40], Ti-6Al-4V parts are first milled and then chemically coated [41]. Resulting surface morphology is schematized on Fig. 3-b from SEM observations Fig. 3-a. Coating is obtained by an industrial and repeatable process, with a chemical bath and subsequent thickness is around 5µm. On the 50-µm scale topography view, a homogeneous 40/60-µm periodic pattern appears. Actually, based on 20-µm observation scale, coating layer is not so homogeneous but composed of clusters whose width is around 4µm. In addition, coating does not cover entirely the substrate, which is confirmed by an EDX analysis. Some cracks due to machining remain visible at the substrate surface.

Composite parts are also milled. SEM observations (Fig. 4-a) have highlighted an anisotropic distribution of glass fibres (Fig. 4-b). The original length of glass fibres is 250-300µm and their diameter is between 10 to 12µm. Additionally, some horizontal fibres have been crushed by milling, what reduces their length to a few dozens of micrometres. The polymer matrix surface aspect is typical for a machining by milling: a periodic pattern appears with some chips.

Contact geometry in considered motor is cylinder-on-pad. So, it was retained on the test bench (Fig. 2-a). Cylinder pin dimensions are 5mm x 10mm with a radius of 30mm (Table 1). Flat pad dimensions are 45mm x 10mm. From the material properties in Table 1 and preload value - 5N -, contact pressure and width are about 8MPa and 70µm respectively, as in real motors.

As it has been above mentioned and detailed in the material test procedure (section 2.3), transparent glass pin will be used in addition to original 1st bodies, in intermediate tests, to observe 3rd body flows inside the contact in operation. In order to minimize the impact on the searched tribological solicitations, chosen transparent material is glass for its chemical similarity with the silica of the coating and the glass fibres of the composite. This choice will be discussed in section 4.3.

2.1.4. Instrumentation

Implemented instrumentation is depicted in Fig. 2-b. Preload force is measured by a strain gauge mounted on a specific deformable test body. Another strain gauge is mounted on the piezoelectric actuator to get its vibratory amplitude. An Eddy current sensor and an accelerometer are used to get the displacement and the acceleration of the moving mass respectively. Friction coefficient is obtained by dividing the monitored acceleration times the mobile's mass by the measured preload force. At last, a camera or high-speed camera are used to see through transparent glass pin when they are used.

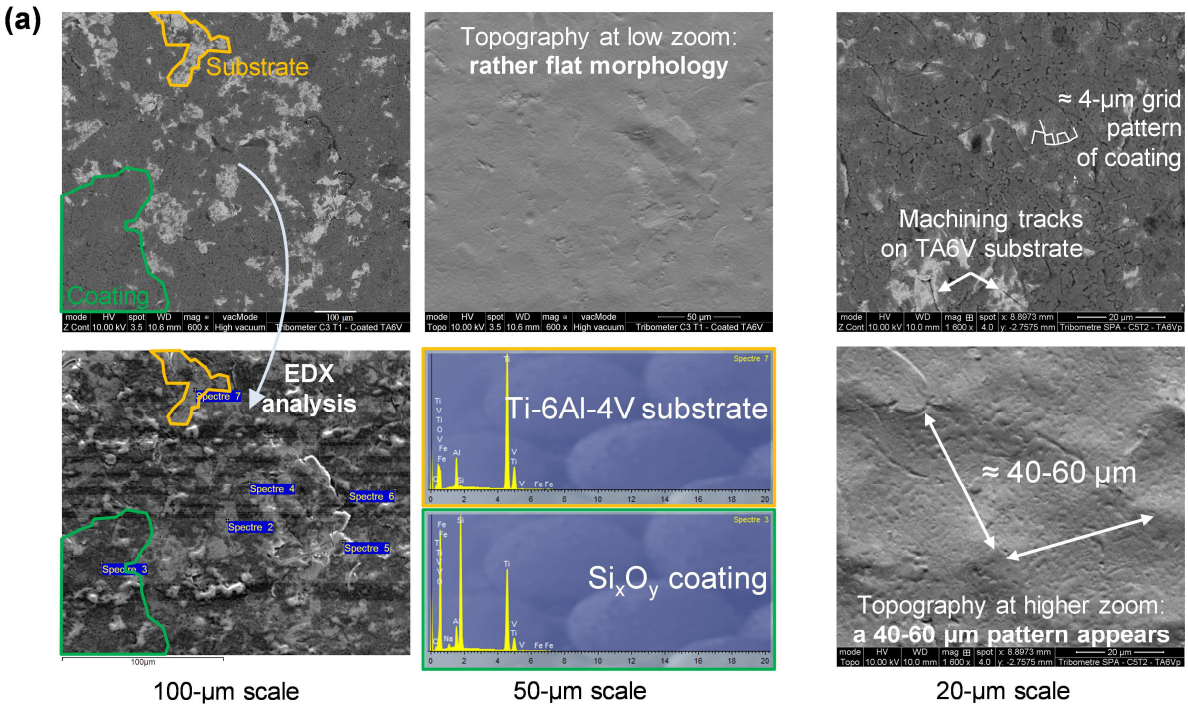

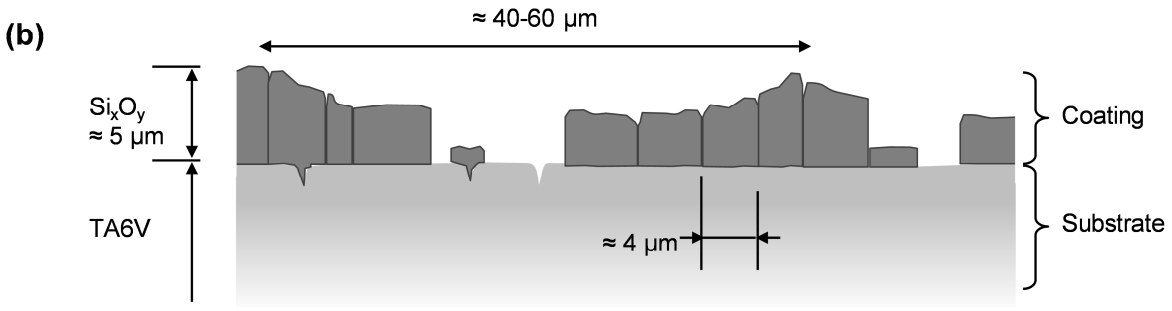

Fig. 3. First body #1: Si_xO_y-coated Ti-6Al-4V [41]. (a) Resulting surface morphology observed by means of Scanning Electron Microscopy and (b) related scheme.

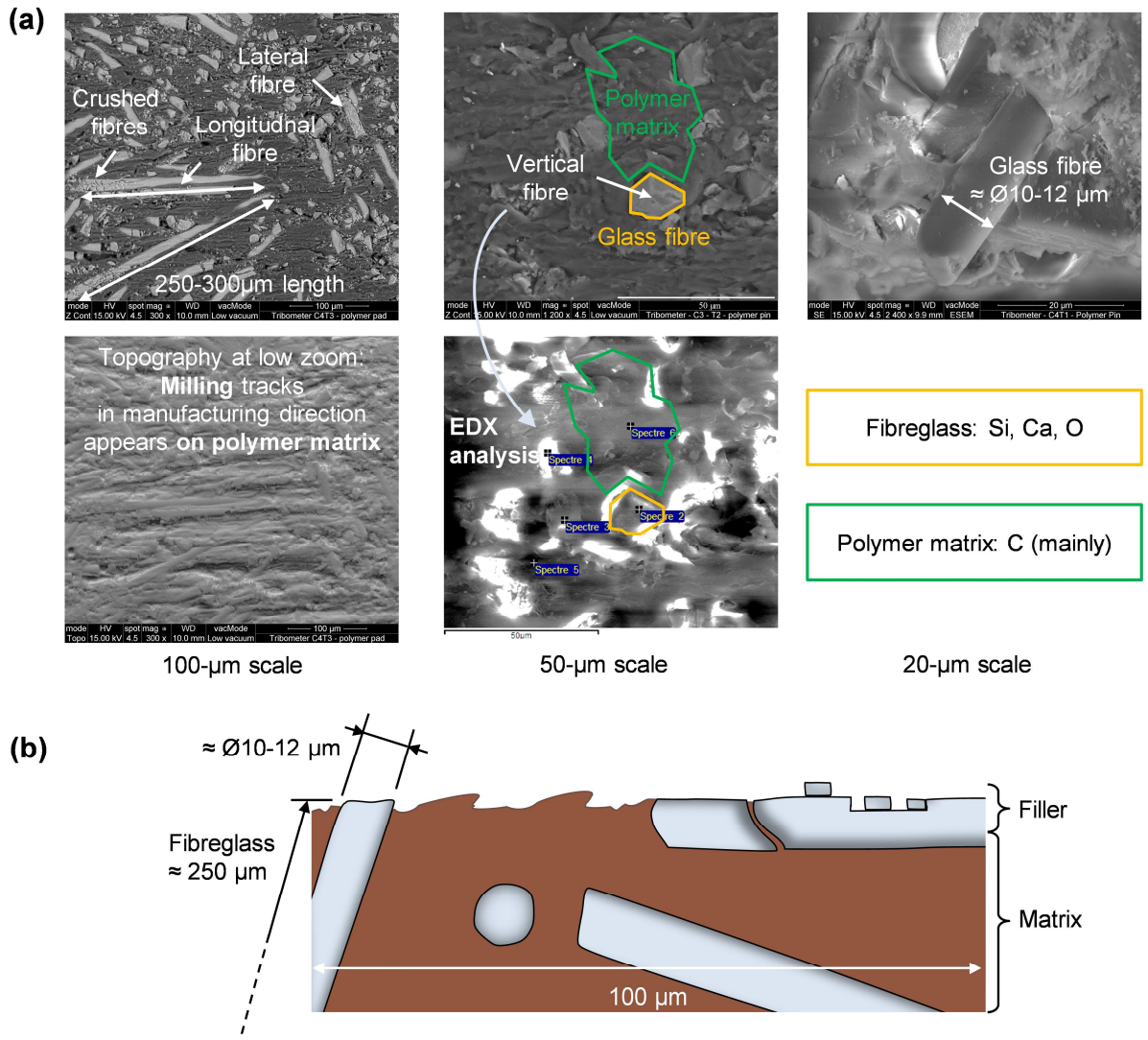

Fig. 4. First body #2: Fiberglass filled composite. (a) Resulting surface morphology observed by means of Scanning Electron Microscopy and (b) related scheme. Notice that EDX analysis is intentionally not disclosed.

2.2. 3rd body experimental framework

The purpose of this work is to deal with tribological issues. At the contact scale, it consists in decrypting the tribological solicitations occurring in the piezoelectric inertia motor by means of a dedicated tribometer. At the mechanism scale, it consists in interpreting friction coefficient evolution and wear generation. Both observation scales are bound by the solid particles flows at the contact interface. In term of methodology, the 3rd body framework is adopted to ensure an objective and reproducible analysis all along the different tests (Fig. 1).

In order to link observed 3rd body morphology to relevant tribological solicitations, it is necessary to describe this morphology in a strictest way. Here, it is realised in four steps.

First *post mortem* observations consist in identifying the observation scale, specific to each considered contact [29, 42]. Here, on the one hand, step size and contact width are around 100-µm order of magnitude. On the other hand, coating height and glass fibre diameter is 10-µm order of magnitude. Each counterpart is so analysed at a macroscopic scale, between 100µm and 500µm. Then, progressive zooms, until 10µm or 5µm, are performed around significant areas. Reference observations (*i.e. ante-mortem*) at both scales must be retained before test for further comparison (Fig. 3 and Fig. 4).

The second part of the analysis consists in defining what a significant area is. To do so, each contact will be divided in three main areas: mean contact area, frontiers, and out-of-frontier. In each of these three areas, purpose is to locate and to characterize significant spots.

Then, spots are described in term of morphology: powdery, ductility, cohesion, compaction, porosity, density, adhesion (SEM), and chemical (EDX) composition. 3rd body volume repartition, punctual presence and preferred orientations, if emerging, are also reported.

Last step consists in linking the position of reported particles to the motion of the friction parts, generated by the motor.. 3rd body flows and velocity accommodation mechanism concepts are then used to formalize what occurs during these events and so to reconstruct the contact life in the form of tribological circuits all along the lifetime of the motor.

2.3. Material test procedure

Experiments were conducted in air environment at around 25°C and 45%rH. Two sequences of material tests were realised:

- the first sequence is carried out with tests operating until around 10^4 operating cycles (20-m equivalent sliding distance) in order to observe the morphology of 3rd body particles after the initiation of 3rd body flows;
- the second sequence is carried out with tests operating at least 10^6 operating cycles (2-km equivalent sliding distance) - initial State-of-the-Art lifetime at the beginning of this work [43] - to get the surface morphology of counterparts after their nominal lifetime.

Each sequence is composed of two tests:

- with fibreglass filled polymer pin on coated Ti-6Al-4V pad;
- with coated Ti-6Al-4V pin on fibreglass filled polymer pad.

Additional tests are carried out *in situ* with a transparent glass pin, for 10^4 cycles, alternatively on fibreglass filled polymer and coated Ti-6Al-4V pads, in order to see solid particle flows in first cycles.

Before considering the different test steps, material samples are systematically cleaned with tension active agents – isopropanol 95% - and optic wipes. Then parts have been dried with clean compressed air.

Next section is based on the previously introduced setup, methodological framework and procedure. It presents the results of the tribological solicitation analyses.

3. Characterisation of tribological solicitations

By stemming from the material test procedure, detailing all the observations, SEM micrographs and monitored data would be cumbersome (experimental procedure flow chart available in supplementary material). Here, purpose is rather to highlight how the chosen method is applied to piezoelectric inertia motor in order to be used on other cases. Thus, only milestones such as *in situ* observations with transparent glass pins (section 3.1) and *post mortem* analyses (section 3.2) are exhibited once, leading to the understanding and to the improvement of this tribological system (section 3.3). Complete analysis can be found in [44].

3.1. In situ analysis: tests with transparent glass pins

Tests with transparent pins are recorded by means of a camera. From the generated videos, significant pictures are extracted and compared to monitoring data (Fig. 5).

Test on coated Ti-6Al-4V pad is firstly described (Fig. 5-b). Then, test on fibreglass filled polymer pad is described (Fig. 5-c). The next two paragraphs are intentionally descriptive. Indeed, interpretations - leading to tribological solicitations - are proposed once the *in situ* analysis is correlated with *post mortem* observations.

From T0 to T1 (Fig. 5-b), contact area materializes by dark particles at the top of observation window: Q_s^i s is activated. Until this step, friction coefficient remains quite low - around 0.2/0.3 -. Some particles move with the amplitude of step size (100µm) whereas some others move with the amplitude of cycle stroke (1mm), both in actuation direction: Q_i is activated. Then, due to contact alignment and wear, particles move in a perpendicular direction - toward the less contact pressure area (section 4.2) -. From T1 to T2, friction coefficient starts to increase from 0.2 to 0.6. Projections of powdered particles appear: Q_e is activated. These particles remain in the range of the cycle stroke (+/-1mm). So, although they are ejected from the contact, they are quickly reintroduced: Q_r is activated. Between T2 and T3, powdered particles agglomerate into clusters. As soon as cluster size overpasses a threshold, they crack and resulting particles are ejected again (Fig. 6. Fig. 6). The major part of these ejected particles is projected far away from the contact and are no more re-introduced: Q_w is activated. In the same time, friction coefficient decreases to around 0.4/0.5. Then, white areas appear. They are suspected to be Ti-6Al-4V substrate. From T3 to T4, some dark areas suddenly lighten and move along actuation direction, typical consequence of a shearing mode [45]. White areas are increasingly present. 3rd body flows activity decreases: particles circulate into the contact, are ejected, reintroduced, and ejected definitely. Simultaneously, friction coefficient stabilises around 0.4.

From C0 to C1 (Fig. 5-c), contact area materializes by shading in the centre of observation window: Q_s^i and Q_i are slowly initiated. Shade area is not homogeneous but seems to superimpose on milling tracks. Until C1, friction coefficient is quite low - around 0.1/0.2 -. From C1 to C2, the size of the shaded area grows. The created 3rd body particles move along actuation direction, with the amplitude of the cycle stroke: they move rather with the pad than with the pin. Therefore, particles, led by the pad, leave the contact and are re-introduced at each cycle: Q_r is activated. Friction coefficient slightly increases to around 0.3/0.4. From C3 to C4, shade area does not grow a lot but becomes more homogeneous. Friction coefficient continues to increase until 0.5. Globally, contrary to the test on coated Ti-6Al-4V, particle motion in other directions than that of actuation was not detected. Likewise, no Q_w was detected.

Thus, 3rd body flows are quite different between these first two tests. With the coated Ti-6Al-4V pad, 3rd body appears rather powdered and quickly leaves the contact, leading to an important Q_w. On the contrary, ductility and adhesion dominate in the 3rd body layer generated from fibreglass filled polymer. *In situ* observations can now be completed with *post mortem* observations on real 1st bodies to get searched contact life.

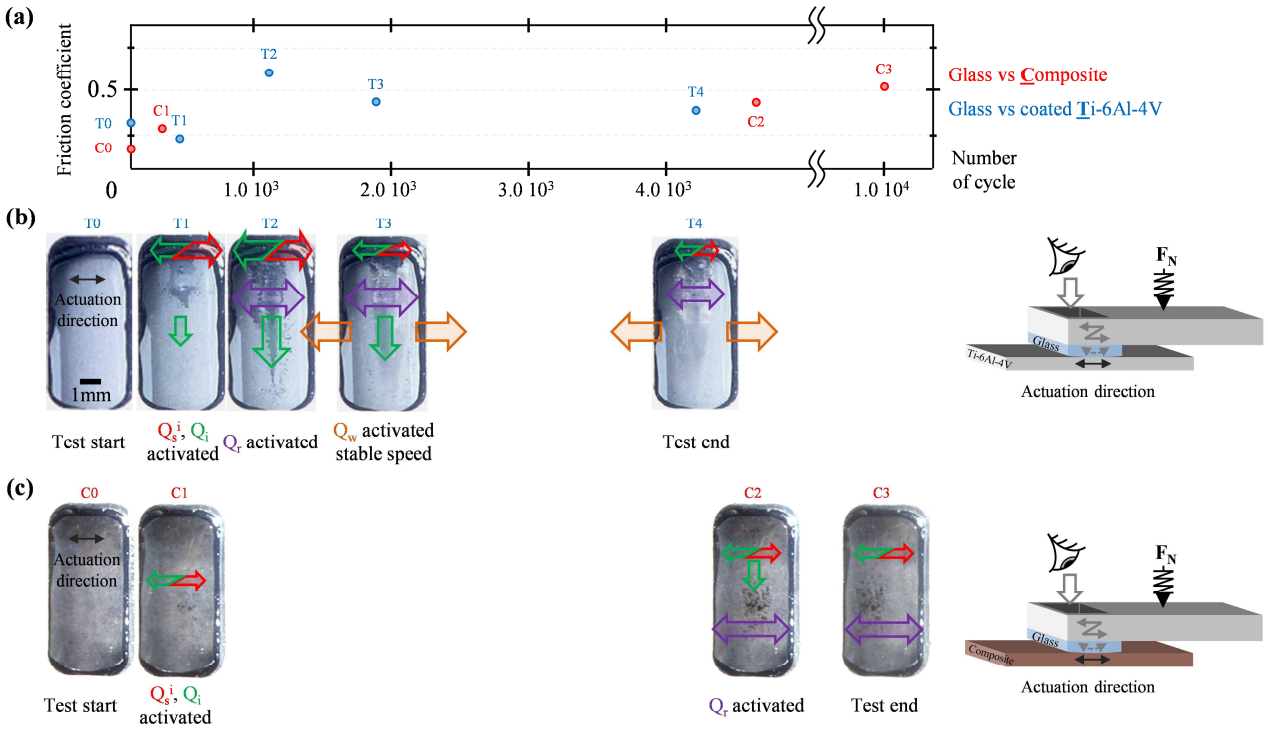

Fig. 5. Tribological timeline of tests with transparent pins to see the 3rd body flows initiation. (a) Friction coefficient evolution extracted at significant *in situ* direct observations. (b) Glass pin / coated Ti-6Al-4V pad contact. (c) Glass pin / fibreglass filled polymer pad contact. (b) and (c) are simultaneously plotted leading to their respective 3rd body flows. Arrow colours are the same as 3rd body flows colour code proposed in nomenclature. The size of arrows represents a rough estimation of the relative 3rd body flow amplitude.

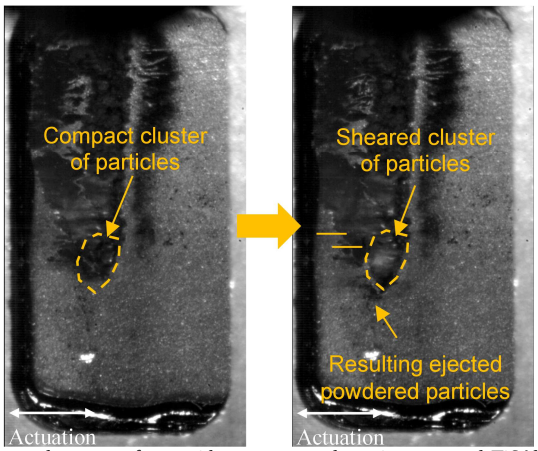

Fig. 6. Successive views stemming from high speed camera of test with transparent glass pin on coated Ti6Al4V pad. During the test, coating particles agglomerate, resulting into dark clusters on the left-hand side picture. Then, as soon as cluster size overpasses a threshold, it cracks, resulting in a sudden clarification of the area on the right-hand side picture. Related particles are powdered and ejected from the contact area.

3.2. Post mortem analyses

From previous analyses, the keys toward the decryption of the contact's life between the fibreglass filled polymer and the coated Ti-6Al-4V starts to emerge. Coating is expected to be quickly detached from the Ti-6Al-4V substrate and entrapped into the ductile layer generated on the composite. This results in (i) a short running-in phase, (ii) a stable 3rd body layer and so (iii) a stable coefficient of friction. These hypotheses have now to be confirmed with *post mortem* analyses. It is illustrated on the case of 10^6-cycles test with fibreglass filled polymer *vs.* coated Ti-6Al-4V. At first trial, test failed before 10^5 cycles. This test, considered as critical, was duplicated to check its reproducibility. Second time, targeted number of cycles was reached and surface morphologies were similar [44]. So, beyond the dispersion on the achieved number of cycles, occurring tribological solicitations are supposed to be the same, leading us to observe the "most worn" test. Once tests are achieved, samples are separated to be analysed with a SEM/EDX (Fig. 7).

The coated Ti-6Al-4V pad is firstly analysed (Fig. 8) followed by the fibreglass filled polymer pad (Fig. 9).

On the macroscopic view (Fig. 8.1), contact area materializes with a homogeneous and smooth 3rd body layer. Powdered particles have been also massively ejected. Ti-6Al-4V substrate areas appears now fully naked, not covered by 3rd body. In addition, plastic grooves appear on 3rd body layer. Fig. 8.2 focuses on the area where Ti-6Al-4V substrate appears. The chips of 3rd body layer are being extruded by shearing (S_3M_3). Free particles coming from coating and from Ti-6Al-4V substrate are observed. Fig. 8.3 focuses on out-of-contact area. It emphasizes the massive volume

of ejected coating particles, whose aspect is very powdered. Fig. 8.4 focuses on the plastic grooves, whose width is between 30 and 70µm and length is longer than 500µm. These plastic deformations could be generated by abrasion, due to the glass fibres on the counterface or by rolling. Their occurrence is rather attributed to rolling (M_4), based on the mechanism (S_0) behaviour. Indeed, the stick-slip actuation would let shorter marks if glass fibres were responsible for scratching these grooves (step size is around 100µm). It remains to find what could generate such grooves by rolling. To do so, a second *post mortem* analysis is accrued out on the fibreglass filled polymer pin (Fig. 9).

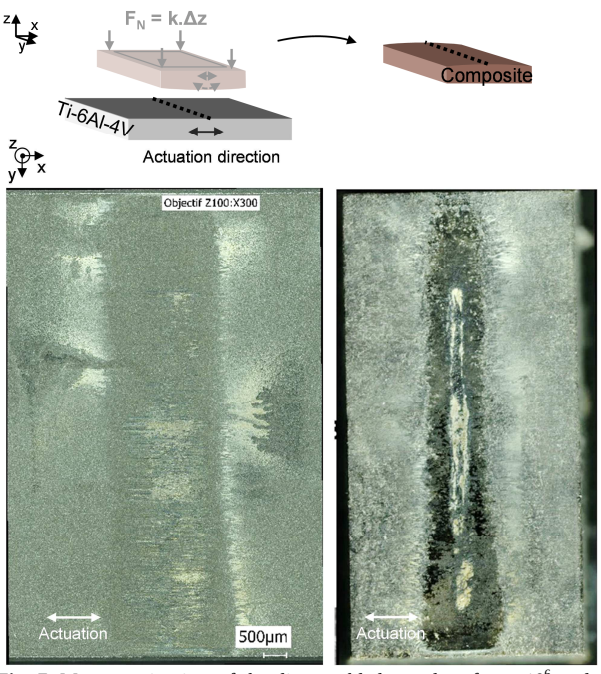

Fig. 7. Macroscopic view of the disassembled samples after a 10^6-cycles test - 2-km equivalent sliding distance - with a fibreglass filled polymer pin vs. coated Ti-6Al-4 pad.

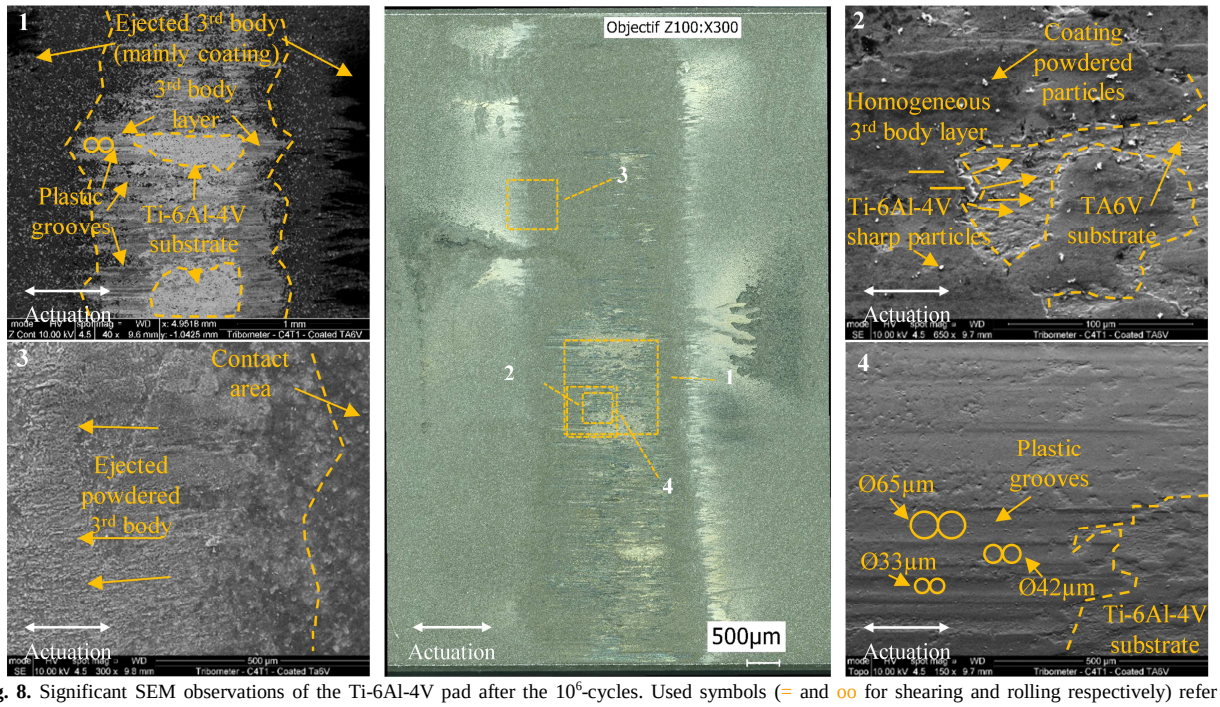

Fig. 8. Significant SEM observations of the Ti-6Al-4V pad after the 10^6-cycles. Used symbols (= and oo for shearing and rolling respectively) refer to accommodation modes introduced in nomenclature.

Fig. 9.1 is achieved by topography microscopy to get the shape of pin surface after test. A triangular "fault" appeared - whose basis is 90-µm width and depth is 50µm -. Early end of first test is attributed to this fault. Indeed, as it is perpendicular to the sliding direction, the stiffness of the pin in this direction is supposed to drastically decrease. Thus, when it is stressed by actuation, elastic deformation due to this normal rupture occurs and accommodates relative displacement (S_1M_2). Back on macroscopic views (Fig. 9.2), areas where fault formed on the composite pin are facing naked Ti-6Al-4V substrate. Thus, fault could be responsible for the massive abrasion of the 3rd body layer and then of the substrate. Fig. 9.3 focuses on the fault. Only vertical glass fibres appear inside. In addition, fault is surrounded by an area without glass fibres. Fig. 9.3 zooms into the fault, focusing on the vertical glass fibres. A 100-µm width composite matrix is being extruded. Pin progressively rubbing, vertical fibres break into fragments and longitudinal crushed fibres leave the matrix. Thus, after a while, there is no more fibres to cement the matrix. Full of holes, it breaks by shearing (S_1M_3). Fault appears. Fig. 9.4 focuses on contact area with empty glass fibre slots. Longitudinal fibres leaving the matrix, are free to roll (S_3M_4) until being broken into fragments. This explains the "grooves" on the Ti-6Al-4V pad.

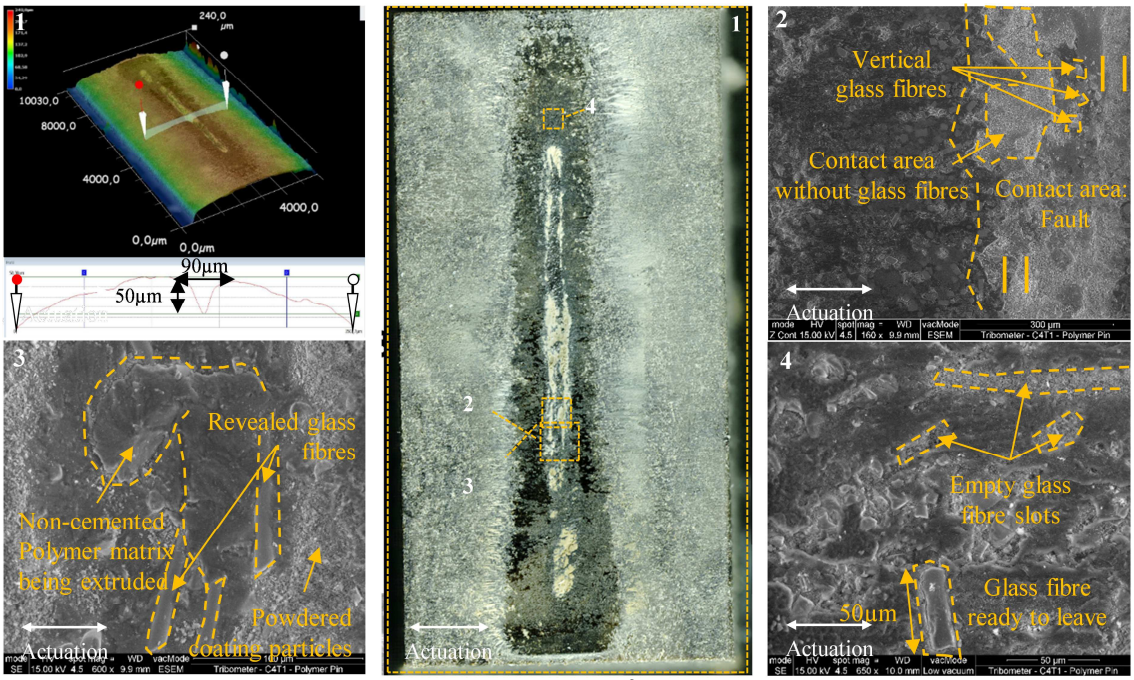

Fig. 9. Significant SEM observations of the fibreglass filled polymer pin after the 10^6-cycles. Used symbol (|| for normal rupture) refers to accommodation mode introduced in nomenclature.

3.3. Tribological circuit: contacts' life

As a synthesis, the tribological circuit of the fibreglass filled polymer pin on coated Ti-6Al-4V pad is proposed in Table 2.

In comparison with test at 10^4 cycles [44], Q_s^i drastically increased, due to the formation of a fault in the composite pin and to the resulting abrasion of counterface. However, the formation of cohesive 3rd body layers on both 1st bodies - mixing coating, glass fibres and polymer matrix - have limited wear flow Q_w. Thus, 3rd body has mainly circulated and recirculated into the contact (Q_i and Q_r).

So, first, a cohesive and abrasive layer forms: Q_s^i and Q_i are activated. Progressively, layer becomes homogeneous: a balance occurs between the different 3rd body flows. Then, the fault starts to appear, increasing roughness and abrading Ti-6Al-4V substrate. Thus, normal rupture starts to partially accommodate relative displacements, leading to an early test end.

Notice that an impact mode - normal separation of the contact - has been observed on other SEM micrographs and measured with a laser vibrometer at the vertical of the pin (Fig. 10). Impacts happen just after the stick phase. So, it can be supposed that wear mechanisms initiate under effect of shearing and impact (M_3+impact).

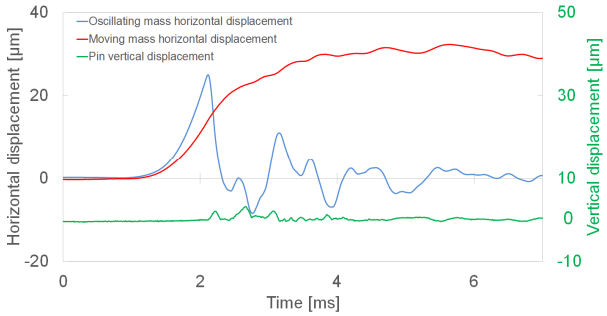

Fig. 10. Measure of contact separations (green curve). Impacts occur after stick-slip transition.

Table 2. Tribological circuit resulting from test analyses with fibreglass filled polymer pin on coated Ti-6Al-4V pad. Accommodation sites and modes in bold are the main ones among those inventoried. Contact-life temporal evolution is deduced from the overlay of contact schemes at different stopped tests.

	3rd body flows				Accommodation	Contact scheme
	Q_s^i	Q_i	Q_e		Sites: S_i Modes: M_j	
			Q_r	Q_w		
Initial state after machining, before test						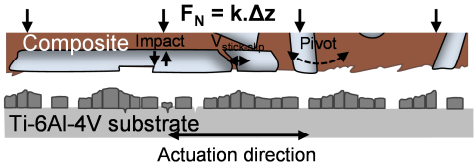
10^4 cycles	++	++	+	+	**S_1: Impact, M_3** S_3: Impact, M_2, **M_3** S_4: Impact, **M_3** S_5: Impact	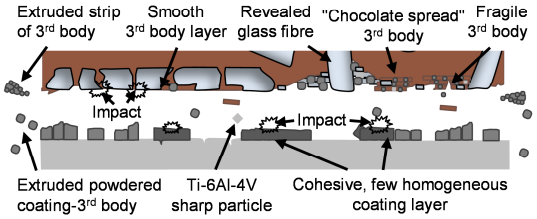
10^6 cycles	++++	+++	+++	++	**S_1:** Impact, **M_2**, M_3 **S_3:** Impact, **M_3**, M_4 S_4: Impact, M_3 S_5: Impact, M_3	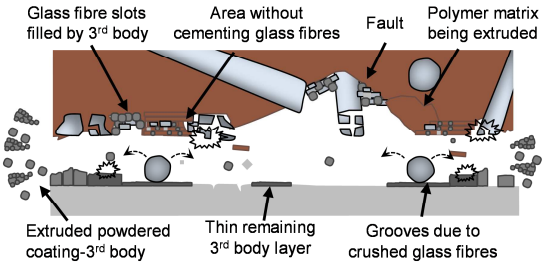

The analysis of this contact highlighted the impact of 1st bodies orientation. Indeed, repeated solicitations on the composite material lead to damage it on a long term. As a result, pursued performances for a long lifetime are not addressed. Thus, it becomes necessary to study the reverse configuration: coated Ti-6Al-4V pin on fibreglass filled polymer pad.

The whole analysis of this contact is proposed in [44]. As a synthesis, the tribological circuit of the coated Ti-6Al-4V pin on fibreglass filled polymer pad is proposed in Table 3.

In comparison with test at 10^4 cycles, the morphologies of both 1st body surfaces are not so different, and so are 3rd body flows. Indeed, lifetime tests last 10^6 cycles against 10^4-cycles tests. So, the volume of mobilized particle is logically more important. However, the amplitude of internal source flow Q_s^i and wear flow Q_w did not change. What is interesting with the test at 10^6 cycles is the amount of coating particles which joined and mixed into 3rsd body layer on the composite surface to cement the free glass fibres fragment resulting from the repeated impacts. Thus, internal flow Q_i and recirculation flow Q_r may slightly increase.

So, as in the reverse contact configuration, first an abrasive layer forms. Then, progressively, 3rd body layer becomes homogeneous: a balance occurs between the different 3rd body flows and friction coefficient slightly decreases. But, contrary the test in the reverse contact configuration, as the 1st body rubbing the most (pin) is in coated Ti-6Al-4V; it does not lead to early failure. In addition, as the 1st body rubbing the less - the composite pad - progressively forms a ductile and cohesive layer from polymer matrix, it leads to trap the different 3rd body particles. This results in a stable and abrasive layer, leading to an important friction coefficient - around 0.5 - stable all along lifetime.

Finally, tests at 10^6 cycles emphasize that, with fibreglass filled polymer and coated Ti-6Al- 4V as 1st bodies, abrasion drives wear mechanisms. When pin is in composite, it results in a quite low wear flow Q_w but in an early test failure due to a normal rupture of the pin. In a reverse configuration, it results in important 3rd body flows leading to a high wear flow Q_w. In this configuration, the ductility of the 3rd body layer formed onto the composite surface makes it possible to trap the most of solid particles, leading to quickly stabilize 3rd body flows amplitudes and so the performances in a long lifetime.

Table 3. Tribological circuit resulting from test analyses with coated Ti-6Al-4V pin on fibreglass filled polymer pad. Accommodation sites and modes in bold are the main ones among those inventoried. Contact-life temporal evolution is deduced from the overlay of contact schemes at different stopped tests.

	3rd body flows				Accommodation	Contact scheme
	Q_s^i	Q_i	Q_e		Sites: Modes: S_i M_j	
			Q_r	Q_w		
Initial state after machining, before test						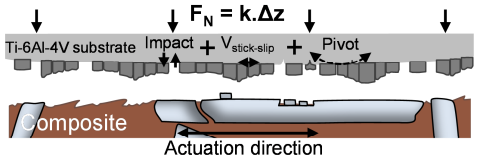
10^4 cycles	+++	+++	++	++	**S_2: Impact, M_3** S_3: M_3 **S_5: Impact, M_3**	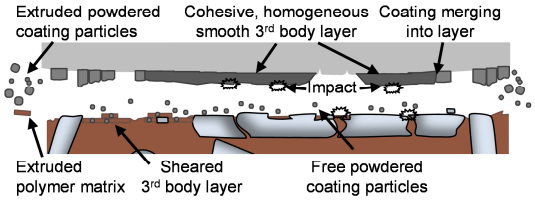
10^6 cycles	+++	++++	+++	++	S_1: Impact, M_3 **S_2: Impact, M_3** **S_3: Impact, M_3**, M_4 S_5: **Impact**, M_3	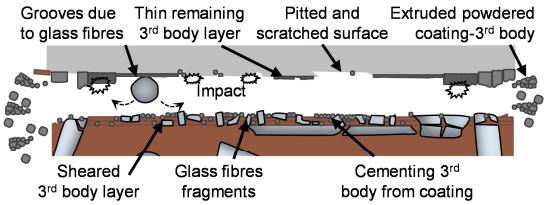

4. Results and Discussion

4.1. Main outcome

From the comparison between the orientation of two 1st bodies, a lifetime test with a coated Ti-6Al-4V pin against a fibreglass filled polymer pad has been achieved. The targeted number of cycles was ten times higher than before: 10^7 cycles/20-km equivalent sliding distance. This test was achieved at first with stable speed performances and successfully reproduced (Fig. 11).

In comparison with 10^6-cycle tests, sudden decreases/increases of mean speed regularly appear after 5.10^6 cycles and an important cohesive wear is observed. We could imagine that, because of its low ductility, the 3rd body layer on composite surface loses its cohesion with repeated stresses. It would lead then to an increase of wear flow Q_w, with the ejection of cohesive particle clusters, in consistence with previous observations. Some substrate area would be then available to be sheared again (S_5M_3). Thus, a new ductile and cohesive 3rd body layer would form. If these results constitute a progress, it should be necessary to lead a similar *post mortem* analysis to confirm the origin of the speed variations.

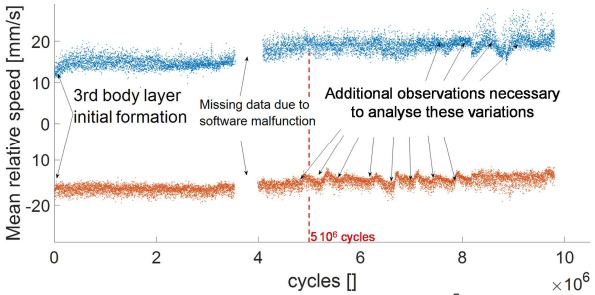

Fig. 11. Mean speed in both actuation direction for a 10^7-lifetime test with coated Ti-6Al-4V pin against fiberglass filled polymer.

4.2. Mechanism effect of test bench in comparison with real motors

Although the introduced tribometer is actuated by a piezoelectric actuator and the contact is preloaded with a spring, some differences with inertia motors remain. In particular, with the tribometer, an impact mode - normal separation of the contact – occurs (Fig. 10). Highlighted by SEM observations and laser measurements, it helps to form the 3rd body layer and to make the performances repeatable. Maybe impacts also occur in inertia motors but it has to be demonstrated. So, it would constitute an interesting perspective. Likewise, now the methodological framework has been set up, it could also rely on the *post mortem* observations of inertia motor to characterize its tribological solicitations directly.

A second difference between the tribometer and reals motors is attributed to the observation window. Impact of this observation window has been assessed by means of an FEM simulation on Abaqus [44]. When there is no observation window, contact pressure is around 7.5MPa along the contact line. Value is consistent with mean/max Hertz contact pressure: 6.9/8.8MPa (Table 1). On the contrary, with the observation window, maximum contact pressure is located on the edges and increases to 9.0MPa. This explains the initiation of 3rd body flow Q_s^i on the top of the window and then, its propagation Q_i toward the centre of the window. Since it has not been done here, it would be interesting to carry out tests without observation window.

4.3. Impact of using intermediate transparent glass pins

The impact of using glass can also be estimated. In its initial state, the surface of glass pin is smooth and volume is stiff and hard. Resulting 3rd body is very powdered. In comparison, 3rd body produced by fibreglass filled polymer and coated Ti-6Al-4V is more ductile-abrasive and cohesive-powdered, respectively. This could explain that the low intensity of 3rd body flows observed in test with glass pin on composite pad is more consistent with the

observations on real 1st bodies than that observed in test with glass pin on coated Ti-6Al-4V pad. Thus, tests with transparent pins bring out crucial information on 3rd body flows but they are not sufficient alone and have to be carried out in synergy with tests on original 1st bodies.

5. Summary and conclusion

The purpose of this work was to characterize tribological solicitations in piezoelectric inertia motors. To achieve such a purpose, a dedicated tribometer has been developed. This tribometer is actuated by a piezoelectric actuator and preloaded with a spring to get closer the behaviour of a real motor. In addition, instrumentation has been implemented to both observe what happens inside the contact by means of a transparent glass pin and to monitor friction coefficient and speed performance evolution. Likewise, an analysis framework - based on 3rd body approach - has been adopted. This framework enabled to compare - by means of *in situ* and *post mortem* observations - different tests with a same methodology to propose systematic analyses, whose conclusions are be less dependent on the observer. This methodology can be summarized in a few points:

- No comparison can be achieved without reference. So, in addition to manufacturing data, when available, first analysis step consists in observing the 1st bodies morphology before tests. To do so, they have to be previously carefully cleaned.
- Second step has consisted in assessing observation scales. Indeed, they differ with the studied mechanisms. In this work, contact and step sizes were around 100µm. Cycle stroke was 1mm. So, first observations were realised at 1-mm scale to get the big picture. Then, progressive zooms below the contact size have been achieved to get morphological changes in comparison with reference observations.
- During the different analyses, parts have been systematically oriented along the actuation direction to be comparable. Then, morphology: cohesion, ductility, powdery, abrasion, porosity, compaction as well as deposit orientations have been assessed. Both have been compared to the inertia motor mechanism behaviour to decrypt the different tribological solicitations.
- Finally, the different observations were formalised by solid particles flows and accommodation sites/modes in a summary table: the tribological circuit.

Based on this methodology, two sequences of tests have been achieved:

- *In situ* observations with glass pins made it possible to observe the chronology of phenomena - such as 3rd body creation and motion - happening during the first operating cycles. These tests made it possible to discover that 3rd body flows coming from coated Ti-6Al-4V were much faster than that coming from fibreglass filled polymer. Thus, powdered coating particles tend to be quickly extruded from the contact, leading to an important wear. On the contrary, fibreglass filled polymer develops a ductile and cohesive 3rd body layer.
- Tests with original 1st bodies - fibreglass filled polymer and coated Ti-6Al-4V - led us to determine that abrasion mainly drives wear flow Q_w and leads to a high friction coefficient - around 0.5 -.

As a conclusion, the characterisation of tribological solicitations stems from above applied methodology: from the first cycles, a 3rd body layer forms on the composite by shearing the carbon matrix. This layer is very ductile and abrasive. It traps broken glass fibres and coating particles. Its propagation is all the more accelerated as its ductility is decreased by the entrapped 3rd body particles. Progressively, Ti-6Al-4V substrate is reached. Related ejected particles join the 3rd body layer, leading to a partial Ti-6Al-4V/Ti-6Al-4V contact. The resulting coefficient of friction is quite high (≈0.5) and remains constant, leading to performance repeatability.

Finally, by replacing the initial - composite pin vs. coated Ti-6Al-4V pad - contact by the reverse configuration: coated Ti-6Al-4V pin vs. composite pad, made it possible to increase the inertia motor lifetime. Indeed, switching the 1st body material is not innocuous. It was induced by the issue of sliding distance. Whereas the pin is always sliding (and wearing), the sliding distance "seen" by the pad depends on the stroke of a cycle (+/-1mm here). So, pad necessarily "sees" less sliding distance. By this way, the lifetime of inertia motors has been multiplied by more than ten, and, above all, without multiplying tests with numerous friction materials.

Acknowledgement

This work was partly supported by the National Association for Research and Technology (ANRT) through the CIFRE convention #2013_1518.

References

[1] A.L.O. Soderqvist. Method and device for displacement of a workpiece, 1973. URL http://www.google.ch/patents/US3957162. US Patent 3,957,162.

[2] G. Lippmann. Principe de la conservation de l'électricité, ou second principe de la théorie des phénomènes électriques (in French). *Journal de Physique Théorique et Appliquée*, pages 381–394, 1881. doi: 10.1051/jphystap:0188100100038100.

[3] Z.-M. Zhang, Q. An, J.-W. Li, and W.-J. Zhang. Piezoelectric friction-inertia actuator - a critical review and future perspective. *The International Journal of Advanced Manufacturing Technology*, pages 669–685, 2012. doi: 10.1007/s00170-011-3827-z.

[4] H. Van Der Wulp. *Piezo-driven stages for nanopositioning with extreme stability: theoretical acpects and practical design considerations*. PhD thesis, Delft University of Technology, 1997.

[5] M. Takano, Y. Tanaka, K. Nakamura, and W. Kaihotsu. The anti-shake, camera shake compensation technology of the α -7 digital (in Japanese). Technical report, Sony, 2005.

[6] T. Morita, R. Yoshida, Y. Okamoto, and T. Higuchi. Three dof parallel link mechanism utilizing smooth impact drive mechanism. *Precision Engineering*, pages 289–295, 2002. doi: 10.1016/S0141-6359(02)00111-3.

[7] R. Buchi, W. Zesch, A. Codourey, and RY. Siegwart. Inertial drives for micro- and nanorobots: analytical study. pages 89–97, 1995. doi: 10.1117/12.228639.

[8] B. L. Blackford, M. H. Jericho, and M. G. Boudreau. A vertical/horizontal two-dimensional piezoelectric driven inertial slider micropositioner for cryogenic applications. *Review of scientific instruments*, pages 2206–2209, 1992. doi: 10.1063/1.1143140.

[9] K. Furutani, T. Higuchi, Y. Yamagata, and M. Mohri. Effect of lubrication on impact drive mechanism. *Precision Engineering*, pages 78 – 86, 1998. doi: 10.1016/S0141-6359(98)00004-X.

[10] C. Belly, H. Mathieu, F. Claeyssen, and RL. Letty. MRI-compliant micro-motors for medical and biomedical applications. Technical report, 2010.

[11] C. Ru, X. Liu, and Y. Sun. *Nanopositioning Technologies: Fundamentals and Applications*. Springer International Publishing, 2016. doi: 10.1007/978-3-319-23853-1.

[12] H. Yoshizawa and J. Israelachvili. Fundamental mechanisms of interfacial friction. 2. stick-slip friction of spherical and chain molecules. *Journal of Physical Chemistry*, pages 11300–11313, 1993. doi: 10.1021/j100145a031.

[13] K.-A. Kounoudji, M. Renouf, G. Mollon, and Y. Berthier. Role of third body on bolted joints' self-loosening. *Tribology Letters*, pages 24–31, 2016. ISSN 1573-2711. doi: 10.1007/s11249-016-0640-8.

[14] M. Godet. The third-body approach: A mechanical view of wear. *Wear*, pages 437–452, 1984. doi: 10.1016/0043-1648(84)90025-5.

[15] H. Czichos, S. Becker, and J. Lexow. Multilaboratory tribotesting: Results from the Versailles Advanced Materials and Standards programme on wear test methods. *Wear*, pages 109–130, 1987. doi: 10.1016/0043-1648(87)90020-2.

[16] A. Bergander, J.M. Breguet, and T. Varidel. Piezoelectric actuator with passive gap for push-pull motion, 2004. URL https://www.google.ch/patents/-WO2004077584A1?cl=en. WO Patent App. PCT/CH2004/000,099.

[17] Peter J. Blau. *Scale Effects in Sliding Friction: An Experimental Study*, pages 523–534. 1992. doi: 10.1007/978-94-011-2811-7_26.

[18] S. Albahrani, D. Philippon, J.-M. Bluet, and P. Vergne. A review of in situ methodologies for investigating EHD contacts. *Proceedings of the Institution of*

Mechanical Engineers, Part J: Journal of Engineering Tribology, pages 86–110, 2015. doi: 10.1177/1350650115590428.

[19] A. Hase, H. Mishina, and M. Wada. Correlation between features of acoustic emission signals and mechanical wear mechanisms. *Wear*, pages 144–150, 2012. doi: 10.1016/j.wear.2012.05.019.

[20] K.J. Wahl, M. Belin, and I.L. Singer. A triboscopic investigation of the wear and friction of MoS_2 in a reciprocating sliding contact. *Wear*, pages 212 – 220, 1998. doi: 10.1016/S0043-1648(97)00246-9.

[21] G. Colas, A. Saulot, C. Godeau, Y. Michel, and Y. Berthier. Decrypting third body flows to solve dry lubrication issue - MoS_2 case study under ultrahigh vacuum. *Wear*, pages 192–204, 2013. doi: 10.1016/j.wear.2013.06.007.

[22] J. Michler, R. Rabe, J.-L. Bucaille, B. Moser, P. Schwaller, and J.-M. Breguet. Investigation of wear mechanisms through in situ observation during microscratching inside the scanning electron microscope. *Wear*, pages 18–26, 2005. doi: 10.1016/j.wear.2005.02.111.

[23] R.-R. Chromik, C.-C. Baker, A.-A. Voevodin, and K.-J. Wahl. In situ tribometry of solid lubricant nanocomposite coatings. *Wear*, pages 1239–1252, 2007. doi: 10.1016/j.wear.2007.01.001.

[24] S. Descartes and Y. Berthier. Rheology and flows of solid third bodies: background and application to an $MoS_{1.6}$ coating. *Wear*, pages 546–556, 2002. doi: 10.1016/S0043-1648(02)00008-X.

[25] H. E. Sliney. Dynamics of solid lubrication as observed by optical microscopy. *ASLE Transactions*, pages 109–117, 1978. doi: 10.1080/05698197808982866.

[26] D Play and M Godet. Visualisation of chalk wear. *The Wear of Non-metallic Materials, Mechanical Engineering Publications, London*, pages 221–229, 1976.

[27] K. J Wahl, R.-R. Chromik, and G.-Y. Lee. Quantitative in situ measurement of transfer film thickness by a newton's rings method. *Wear*, pages 731–736, 2008. doi: 10.1016/j.wear.2007.04.009.

[28] T.-W. Scharf and I.-L. Singer. Quantification of the thickness of carbon transfer films using raman tribometry. *Tribology Letters*, pages 137–145, 2003. doi: 10.1023/A:1021942822261.

[29] P. Stoyanov, H. W. Strauss, and R. R. Chromik. Scaling effects between micro- and macro-tribology for a ti-mos_2 coating. *Wear*, pages 149 – 161, 2012. doi: 10.1016/j.wear.2011.08.021.

[30] I.-L. Singer, S.-D. Dvorak, K.-J. Wahl, and T.-W. Scharf. Third body processes and friction of solid lubricants studied by in situ optical and raman tribometry. *Tribology Series*, pages 327–336, 2002. doi: 10.1016/S0167-8922(02)80036-0.

[31] S.-D. Dvorak, K.-J. Wahl, and I.-L. Singer. In situ analysis of third body contributions to sliding friction of a Pb-Mo-S coating in dry and humid air. *Tribology letters*, pages 263–274, 2007. doi: 10.1007/s11249-007-9270-5.

[32] B. A. Krick, J. R. Vail, B. N. J. Persson, and W. G. Sawyer. Optical in situ micro tribometer for analysis of real contact area for contact mechanics, adhesion, and sliding experiments. *Tribology Letters*, pages 185–194, 2012. doi: 10.1007/s11249-011-9870-y.

[33] A. Jullien, M.H. Meurisse, and Y. Berthier. Determination of tribological history and wear through visualisation in lubricated contacts using a carbon-based composite. *Wear*, pages 116 – 125, 1996. doi: 10.1016/0043-1648(95)06813-9.

[34] S. Fayeulle, P.D. Ehni, and I.L. Singer. *Paper V (ii) Role of transfer films in wear of MoS_2 coatings*. Tribology Series. 1990. doi: 10.1016/S0167-8922(08)70249-9.

[35] T.-W. Scharf and I.-L. Singer. Role of third bodies in friction behavior of diamond-like nanocomposite coatings studied by in situ tribometry. *Tribology transactions*, pages 363–371, 2002. doi: 10.1080/10402000208982561.

[36] F. Dubois, C. Belly, A. Saulot, and Y. Berthier. Design of a dynamic tribometer applied to piezoelectric inertia drive motors - in situ exploration of stick-slip principle -. *Tribology Online*, pages 218–226, 2016. doi: 10.2474/Trol.11.218.

[37] D. Tonazzi, F. Massi, A. Culla, L. Baillet, A. Fregolent, and Y. Berthier. Instability scenarios between elastic media under frictional contact. *Mechanical Systems and Signal Processing*, pages 754–766, 2013. doi: 10.1016/j.ymssp.2013.05.022.

[38] F. Dubois, C. Belly, A. Saulot, and Y. Berthier. Stick-slip in stepping piezoelectric inertia drive motors – mechanism impact on a rubbing contact. *Tribology International*, 2016. doi: 10.1016/j.triboint.2016.04.008.

[39] Z. Rihova, V. Stary, and L. Bacakova. A study of the structure and surface properties of nanostructured biocompatible coatings on Ti alloys. *Vacuum*, pages 630 – 633, 2012. doi: 10.1016/j.vacuum.2011.07.007.

[40] A. Merstallinger and M. Sales. Cold welding due to impact and fretting under vacuum. considering scaling for applications in space mechanisms. *Mechanical Properties Of Complex Intermetallics*, pages 191–248, 2011. doi: 10.1142/9789814322171_0006.

[41] A. Baumann and N. Zander. Ti6Al4V with anodization type II: Biological behavior and biomechanical effects. Technical report, DOT America, 2005.

[42] Satish Achanta, T Liskiewicz, Dirk Drees, and J-P Celis. Friction mechanisms at the micro-scale. *Tribology International*, pages 1792–1799, 2009. doi: 10.1016/j.triboint.2009.04.018.

[43] C. Belly. *Moteurs piézoélectriques inertiels: conceptions, réalisations, test et applications (*in French*)*. PhD thesis, Université de Technologie de Belfort-Montbeliard, 2011.

[44] F. Dubois. *Tribological and vibratory approaches for amplified piezoelectric inertia motors (in preparation)*. PhD thesis, Institut National des Sciences Appliquées de Lyon (INSA), 2017.

[45] Y. Berthier. Experimental evidence for friction and wear modelling. *Wear*, pages 77–92, 1990. doi: 10.1016/0043-1648(90)90210-2.

Supplementary material

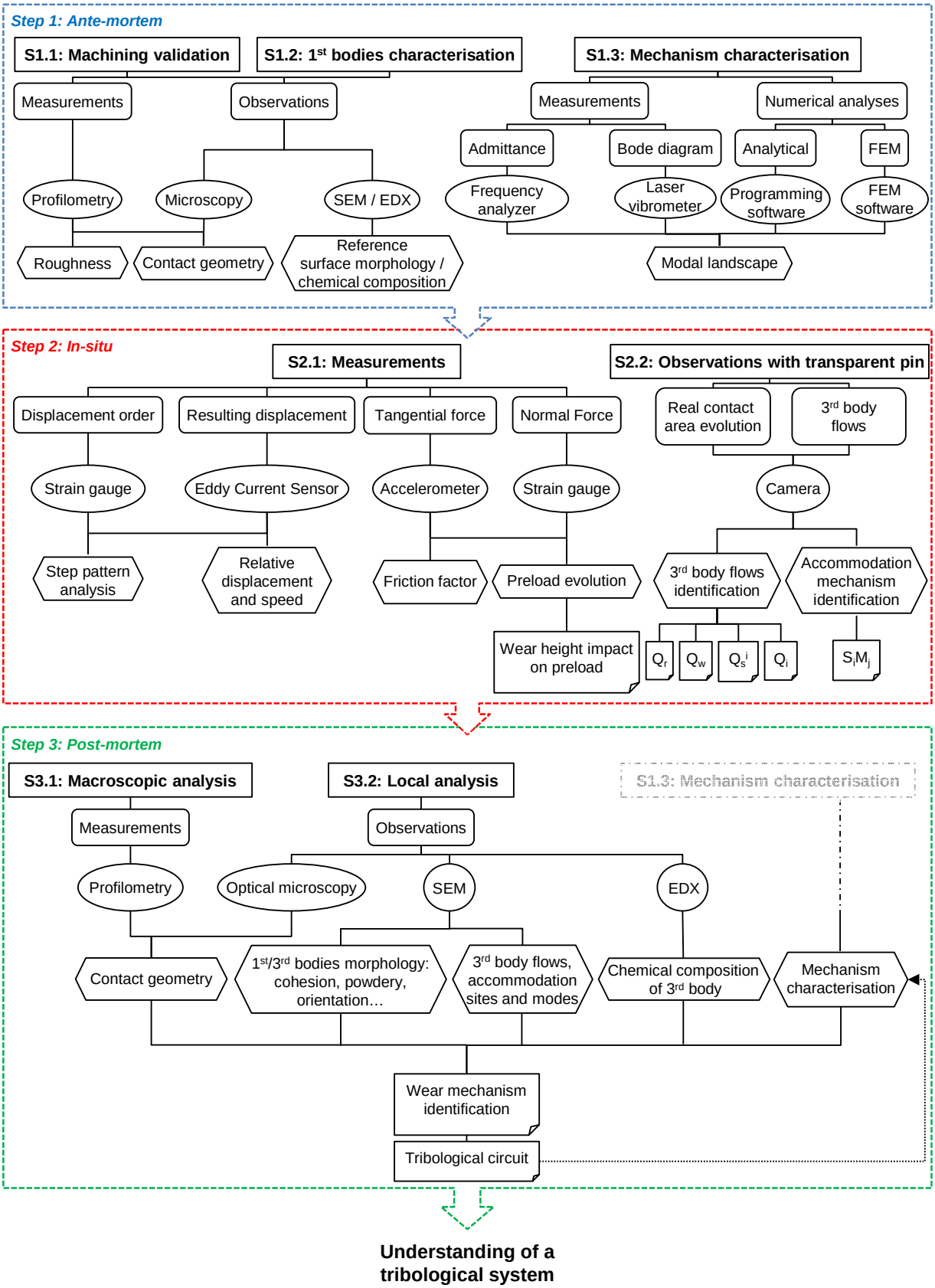

Supplementary fig. Tribological procedure. Each step - dashline frame - is structured with substeps - rectangle -, performed in sequences - oblong -, with tools - ellipse -, leading to results - diamond -, and thus to conclusions - post-it note -.